J Solid State Electrochem (2014) 18:1307–1317
DOI 10.1007/s10008-013-2314-x

ORIGINAL PAPER

PtM/C (M=Ni, Cu, or Ag) electrocatalysts: effects of alloying components on morphology and electrochemically active surface areas

V. E. Guterman · T. A. Lastovina · S. V. Belenov · N. Yu. Tabachkova · V. G. Vlasenko · I. I. Khodos · E. N. Balakshina

Received: 21 July 2013 / Revised: 9 October 2013 / Accepted: 23 October 2013 / Published online: 21 November 2013

Abstract The microstructures of Pt/C and PtM/C (M=Ni, Cu, or Ag) electrocatalysts were studied using X-ray diffraction and transmission electron microscopy (TEM). The electrochemically active surface areas of the prepared materials were estimated by cyclic voltammetry in 1 M H_2SO_4. The materials, with metal contents ranging from 30 to 35 wt.%, were synthesized by chemically reducing the metal precursors in water–ethylene glycol solutions. The actual composition of the bimetallic nanoparticles corresponds to a theoretical (1:1) composition for the PtAg/C catalysts, whereas in the PtNi/C and PtCu/C materials, a portion of the alloying component exists in an oxide form. Decreasing the average metallic crystallite sizes from 3.5 to 1.6 nm does not increase the electrochemically active surface area. This apparent contradiction is because a majority of the PtNi and PtCu nanoparticles consist of 2–4 disordered crystallites. In addition, a portion of the PtNi or PtCu nanoparticle surface is covered by nickel or copper oxides, respectively. PtAg nanoparticles, which have a smaller size relative to other bimetallic particles according to the TEM data, are characterized by an intense platinum surface segregation. The agglomeration processes are lowest for the PtAg nanoparticles.

Keywords Electrocatalysis · Catalyst · Pt/C · Pt alloys · Oxygen electroreduction · Nanoparticles · Crystallites · CO chemisorption · Fuel cell

V. E. Guterman (✉) · T. A. Lastovina · S. V. Belenov
Chemistry Department, Southern Federal University, Zorge St. 7, 344090 Rostov-on-Don, Russia
e-mail: gut57@mail.ru

N. Y. Tabachkova
National University of Science and Technology (MISIS), Moscow, Russia

V. G. Vlasenko
Institute of Physics, Southern Federal University, Rostov-on-Don, Russia

I. I. Khodos
Institute of Microelectronics Technology and High Purity Materials RAS, Chernogolovka, Russia

E. N. Balakshina
Institute of Physical and Organic Chemistry, Southern Federal University, Rostov-on-Don, Russia

Introduction

Pt/C materials are the most effective catalysts for methanol and hydrogen–oxygen low temperature fuel cells [1]. The primary limitations to the commercialization of these catalysts are the high cost of platinum and the rapid catalyst degradation that occurs during operation. The last phenomenon is more common in the oxygen electrode. Efforts to overcome these difficulties can be classified as follows: (1) developing techniques to control particle sizes and to decrease the Pt nanoparticle size distribution [2–4], (2) developing techniques to control particle shapes to increase the surface areas of the active catalytic facets [5–7], and (3) developing platinum alloys with several *d*-metals to increase the specific activity of the catalyst [1, 7–10]. There has recently been interest in preparing multicomponent nanoparticle electrocatalysts with complex structures. The nanoparticle surface is formed by atoms of stable and catalytically active metals (platinum),

and the core consists of non-precious metal atoms [10–16]. The search for new types of supports that combine electrical conductivity with higher corrosion resistance than carbon powders [15–19] can be considered as a separate research area with particular importance for the oxygen electrode.

Optimizing the compositions and microstructures of catalysts requires appropriate experimental methods. X-ray diffraction (XRD) is one of the easiest and most commonly used methods for investigating the structural properties of PtM/C catalysts [1, 18]. The Scherrer equation can be used to estimate the average crystallite size [18]. For catalysts that contain bimetallic solid-solution PtM nanoparticles, the alloying efficiency (extent of alloying) can be estimated using Vegard's law [1, 18–23]. Unfortunately, these estimations of the crystallite and nanoparticle sizes are not always correct. Moreover, to determine the true catalytic surface area, one must account for the particle size distribution and the existence of a greater or lesser number of junctions and agglomerates formed from nanoparticles. Nanoparticles that have limited access for reagents cannot function as effective electrocatalysts. This situation can occur, for example, when nanoparticles are located in the small pores of a carbon support.

Transmission electron microscopy (TEM) is the only technique that can be used for directly observing nanoparticles. However, TEM is a local technique that can only collect particle size information over a very small area. Unfortunately, the spatial distribution of nanoparticles and the degree of their agglomeration may differ for different parts of the support surface. Hence, the choice of one or another part of the support surface for microscopic examination does not always provide an objective result.

As shown in Table 1, electrocatalysts with similar microstructural characteristics possess a variety of active surface area values.

Electrochemical techniques are usually employed to estimate the electrochemically active surface area (ECSA) of a catalyst. Cyclic voltammetry is a commonly used technique, and it is based on the electrochemical oxidation of chemisorbed CO or an electrochemical adsorption analysis (underpotential deposition) and the desorption of monolayers of hydrogen, copper, and so on. [24–32]. For catalysts with high metal loadings (>20 wt.%), the ratio between the ECSA and the geometric surface area (Sg), which can be calculated using simple geometrical models, is less than 1 as a rule.

The ECSA/S_g ratio is often used as a parameter to measure the efficiency of catalysts and the catalytic layer microstructure. Note that the ECSA values determined in references [25] and [30] (Table 1) are overestimated because even a simple calculation based on the ideal model of non-overlapping spheres yields ECSA values of less than 70 and 47 $m^2*g_{Pt}^{-1}$, respectively.

Table 1 An average nanoparticle size, calculated by using TEM and XRD data, and the electrochemical active surface area (ECSA) for Pt, Pt_xNi, and Pt_xCo catalysts

Catalysts composition	Pt loading, % wt/wt	An average nanoparticle size, nm [1]XRD; [2]TEM data	ECSA, $m^2*g_{Pt}^{-1}$	Reference number
Pt_3Co/C (E-TEK)	16.4±0.3	4.2[1]	78±16	25
Pt_3Co/C (TKK)	46.1±0.6	4.0[1]	80±16	25
Pt/C (E-Tek)	40	3.0[2]	12.6	26
Pt/C	40	1.7±0.4[2]	22.3	26
Pt_3Co/C	40	2.0±0.2[2]	22.9	26
Pt_3Ni/C	40	3.6±0.9[2]	23.0	26
Pt_2Ni/C	40	3.1[1]	44.3	27
Pt_3Ni_2/C	40	3.2[1]	38.1	27
PtNi/C	40	3.0	36.4	27
Pt_5Ni/C	20	3.1±1.4[2]	44.7	28
Pt_3Ni/C	20	2.8±1.2[2]	55.4	28
Pt_2Ni/C	20	2.4±1.1[2]	54.9	28
PtNi/C	20	2.3±1.3[2]	44.9	28
Pt/C	20	2.2[1]	88.81	29
Pt_5Co/C	20	2.5[1]	70.48	29
Pt_3Co/C	20	2.4[1]	63.99	29
Pt_2Co/C	20	2.2[1]	54.82	29
PtCo/C	20	2.5[1]	56.61	29
Pt/C	40	6.1[1]	65.2	30
Pt_4Co/C	40	6.0[1]	51.4	30
Pt_3Co/C	40	6.2[1]	47.7	30
Pt_2Co/C	40	6.1[1]	41.5	30
PtCo/C	40	6.1[1]	38.3	30

From the above discussion, it can be concluded that developing an electrocatalyst with a high ECSA requires specific synthesis conditions and a particular metal nanoparticle composition (in the case of Pt alloys), which could provide a combination of optimal[1] nanoparticle sizes with a minimal degree of sintering.

The aim of this study was to compare the microstructure parameters and ECSAs of Pt/C and bimetallic PtM/C catalysts (M=Ni, Cu, or Ag) prepared through a chemical reduction of metal ions from water–ethylene glycol solutions [23, 24]. It was necessary to first establish a correlation between the average crystallite size and the electrochemically active electrocatalyst surface

[1] The specific catalytic activities of Pt and its alloys ($A*m^{-2}$) decrease if the nanoparticle diameter is less than 2–3 nm. The consequence of this effect is the extreme dependence of mass activity ($A*g_{Pt}^{-1}$) on the catalyst ECSA [1, 7].

area, which depends on the nature of the alloying component of the PtM nanoparticles.

Experimental

Pt/C, PtNi/C, PtCu/C, and PtAg/C were prepared by chemically reducing the metal precursors (H_2PtCl_6*$6H_2O$, Aurat, Moscow, Russia) from a carbon suspension based on water–ethylene glycol solvents. The synthesis technique is described in detail in a previous publication [23]. Vulcan XC-72 (which has a specific surface area of 250–280 m^2*g^{-1}) was used as the carbon support. The carbon suspension was prepared such that the complete reduction of the metal precursors yielded an alloy with a Pt:M molar ratio of 1:1 and a metal content of 30 wt.% in the catalyst. A 0.5 M solution of $NaBH_4$ was used as a reducing agent; an excess of $NaBH_4$ was added to the carbon suspension of metal precursors at 25 °C under intensive stirring. The preliminary suspension was ultrasonically stirred. The prepared catalyst powders were separated by suspension filtration using a Buchner funnel, washed with acetone and water, and dried at 100–120 °C for 3 h. Diffraction patterns for the Pt/C and PtM/C materials were obtained at room temperature using an ARL X'TRA (Thermo Scientific, Switzerland) diffractometer with CuKa radiation (λ=0.154056 nm). The diffraction patterns were recorded between $30°\leq 2\theta \leq 95°$ using the step scanning mode with a step of 0.02° 2θ and an exposure time of 4 s per step.

The X-ray reflections were fitted using the WinPLOTR program of the FullProf software suite [33]. The reflections from the synthesized samples were fitted by accounting for reflections corresponding to the carbon support [34, 35]. The average particle size was determined using the well-known Scherrer equation as follows: $\overline{D} = K\lambda/(FWHM\cos\theta)$, where λ is the wavelength, $\overline{D}$ is the volume-averaged particle size, K=0.89 is Scherrer constant, FWHM is full width at half maximum, and θ is Bragg angle of the [*hkl*] reflection. The Scherrer equation is a simple method for calculating the average nanoparticle size using recently reported results [34–37], which revealed that more precise calculation methods do not have a significant effect on the value of $\overline{D}$.

The Ni*K*- and PtL_3-edges of the EXAFS spectra for the PtNi/C sample were obtained at the "Structural Materials Science" Station K1.3b at the Kurchatov Center for Synchrotron Radiation and Nanotechnology (Moscow, Russia) [37]. A storage ring with an electron beam energy of 2.5 GeV and a current of 70–90 mA was used as the radiation source. All of the spectra were recorded in transmission mode using a channel-cut Si (111) monochromator, and two N_2- or Ar-filled ionization chambers were used as detectors. The EXAFS data were analyzed using the IFEFFIT data analysis package [38]. The reduction of the EXAFS data was performed following standard procedures for pre-edge subtraction and spline background removal.

Radial pair distribution functions around the Ni and Pt ions were obtained by Fourier transformation of the k^3-weighted EXAFS functions over the range of photoelectron wavenumbers 2.5–13.0 $Å^{-1}$. The structural parameters, including interatomic distances (R), coordination numbers (CN), and the distance mean-square-deviation Debye–Waller factors (σ^2), were determined from a nonlinear fit of the theoretical spectra to the experimental spectra. The experimental data were simulated using theoretical EXAFS amplitudes and phase functions, which were calculated using the FEFF7 program [39]. The amplitude reduction factor, S_0^2, and the threshold energy, E_0, were calibrated by fitting the EXAFS data with the model compound-metal foils. The amplitude reduction factor, S_0^2, was found to be equal to 0.9 in all cases. The quality of fit was estimated from discrepancy factors between the experimental and simulated functions (Q-factor).

TEM analysis was performed using a JEM-2100 (JEOL, Japan) microscope operated at an accelerating voltage of 200 kV. The catalyst powders were placed in heptane to prepare the samples for TEM analysis. The suspension was then ultrasonically dispersed, and one drop of the suspension was deposited onto a copper grid sputter-coated with carbon.

The active surface area was determined on a stationary electrode using the cycling voltammetry method. Measurements were performed in three-electrode cells at room temperature; a saturated silver chloride electrode was used as the reference electrode. All potentials in this work are referenced versus a standard hydrogen electrode. A 1 M H_2SO_4 solution saturated with Ar at atmospheric pressure was used as an electrolyte.

An aliquot (20 μl) of catalytic ink was applied to the surface of a glassy carbon electrode and dried at 80 °C for 40 min to form a thin catalyst layer on the electrode surface. The catalytic ink consisted of a dispersed suspension of 0.014 g of electrocatalyst in a 2-ml mixture, which was prepared by mixing 20 ml of isopropanol, 70.8 ml of water, and 2 μl of a 10 % Nafion solution.

Before measuring the active surface area, the electrode surface was standardized. For this purpose, the electrolyte was purged with argon for 40 min, and then it was cycled (25 cycles) at a potential range from 0.042 to 1.192 V, with a potential scan rate of 100 mV*s^{-1}. To determine the active surface area of the metals by accounting for the amount of electrochemically oxidized chemisorbed CO, a constant electrode potential of 0.47 V was maintained and the electrolyte

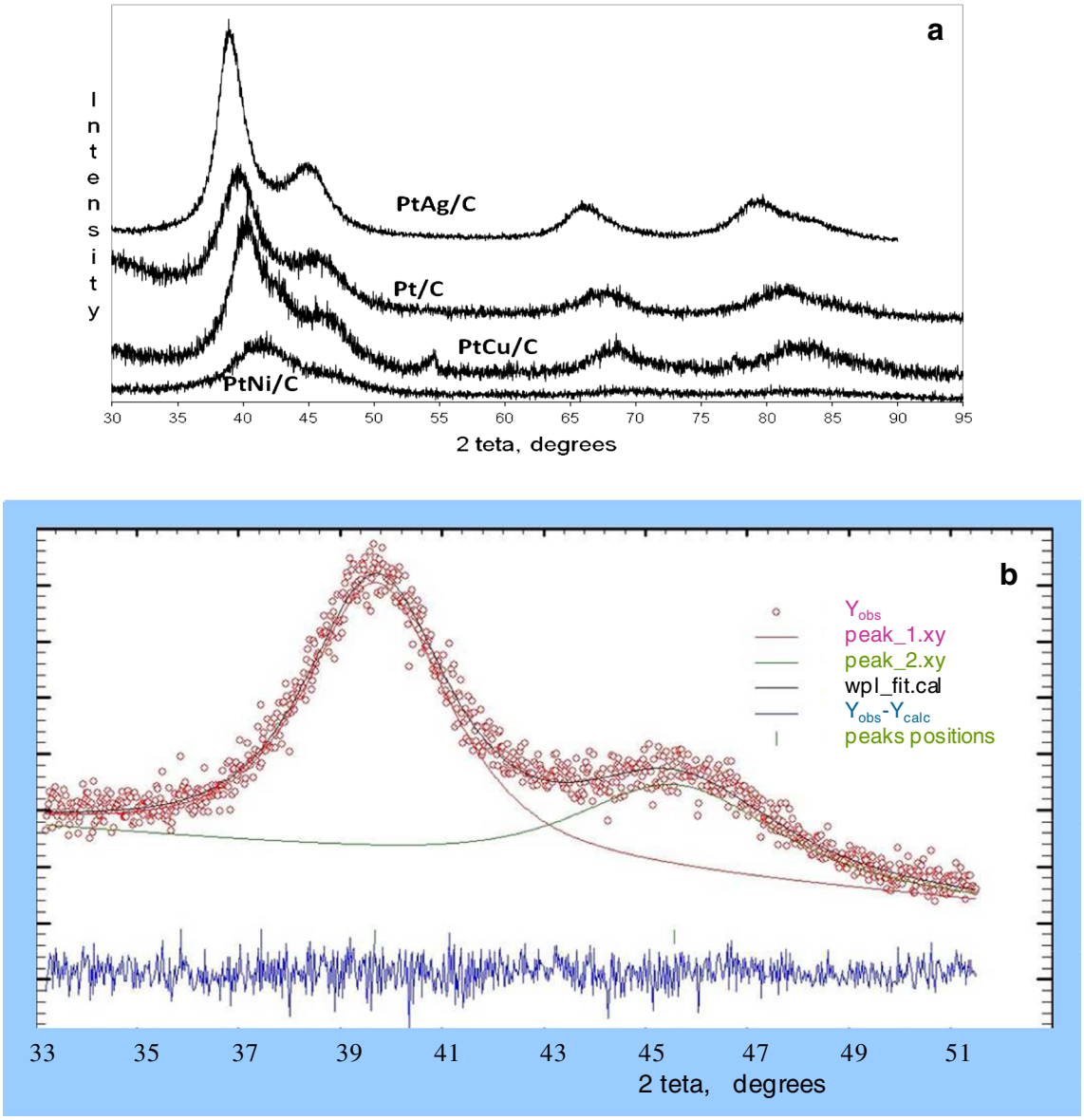

Fig. 1 X-ray diffraction patterns for the synthesized Pt/C, PtNi/C, PtCu/C, and PtAg/C electrocatalysts (**a**) and 111 and 200 reflex approximations for Pt/C (**b**)

Table 2 Synthetic electrocatalyst characteristics

Sample	Material composition			Metal's loading in the catalyst, % wt/wt		2θ, deg.	FWHM, deg.	Lattice parameter, nm	Average size of crystallites, nm
	Phase composition	Pt: M mole ratio in the catalyst by the results of X-ray fluorescent analysis	Pt: M mole ratio in the alloy (calculated by the Vegard's law)	Calculated	Experimental				
Pt/C	Pt, C	–	–	30	31	39.65	4.2	0.3934	2.1
PtNi/C	Pt(Ni)[a],C	$Pt_{42}Ni_{58}$	$Pt_{61}Ni_{39}$	35	33	41.50	5.6	0.3808	1.6
PtCu/C	Pt(Cu)[a], CuO, C	$Pt_{46}Cu_{54}$	$Pt_{82}Cu_{18}$	30	30.2	40.27	4.52	0.3876	2.0
						CuO: 42,51 (refl. 200)	–	0.2464	–
PtAg/C	Pt(Ag)[a],C	$Pt_{56}Ag_{44}$	$Pt_{51}Ag_{49}$	31	32	39.02	2.34	0.4003	3.8

[a] Designation Pt(M) corresponds to the phase of the platinum-based solid solution

Table 3 EXAFS fitting parameters at the PtL_3-edge and NiK-edge for NiPt/C

Sample	Shell	CN	R, Å	σ^2, Å^2
NiPt/C	Ni-O/C	2.0	1.85	0.0045
NiK-edge	Ni-O/C	1.0	1.97	0.0045
	Ni-Ni	1.4	2.49	0.0053
	Ni-Pt	1.5	2.63	0.0060
NiPt/C	Pt- O/C	0.7	1.91	0.0050
PtL_3-edge	Pt-Ni	1.7	2.63	0.0052
	Pt-Pt	4.5	2.69	0.0060
Pt-foil	Pt-Pt	12	2.75	0.0060
Ni-foil	Ni-Ni	12	2.49	0.0050

CN coordination number, *R* bond distance, σ^2 Debye–Waller factor

was sequentially purged with CO for 20 min and then with argon for 40 min. Next, the cyclic voltammogram (CV) (3 cycles) was measured over a potential range of 0.042 to 1.192 V, with a potential scan rate of 40 mV*s^{-1}. To determine the active surface area from the amount of adsorbed and/or desorbed hydrogen, the electrolyte was purged with argon for 40 min, and then the CVs (25 cycles) were measured over a potential range of 0.042 to 1.192 V, with a potential scan rate of 100 mV*s^{-1}.

The following equation was used to calculate the active surface area of the metal catalyst components:

$$ECSA = Q/[R \times L] \quad (1)$$

ECSA is the active surface area of an alloy or platinum in square centimeter per gram, Q is the charge corresponding to the peak of CO oxidation in the CV or to the region of hydrogen desorption (or half of the sum for the regions of hydrogen adsorption and desorption) minus the contribution of the double layer region in microcoulomb, R is the charge consumed for the electrochemical conversion of a hydrogen or CO monolayer, which is 210 and 420 μC*cm^{-2}, respectively, and L is the alloy or platinum loading on the electrode in grams.

Results and discussion

The prepared Pt/C and PtM/C are composites that contain metal components in a nanoparticle form. The nanoparticle status is evidenced by the presence of broad peaks in the X-ray diffractograms of these materials (Fig. 1).

In the case of binary materials, broadening of the diffraction peaks could be caused not only by small nanoparticles but also by their nonuniform composition and by superposition of peaks corresponding to different phases. To identify any possible superposition of the peaks of different phases, the X-ray diffractograms were fitted while considering the contribution of the carbon support reflections (Fig. 1b). For the Pt-M alloys (solid solutions), the peaks shifted to larger (for PtCu and PtNi) or smaller (PtAg) angles (2θ) compared to those for pure platinum (Fig. 1a). The lattice parameters of the binary materials (Table 2), which were calculated from the X-ray diffraction data, confirmed the formation of substitutional solid solutions. The formation of that solution causes deviations in the observed parameters from the given values, which are typical for pure platinum nanoparticles (a=0.3934 nm).

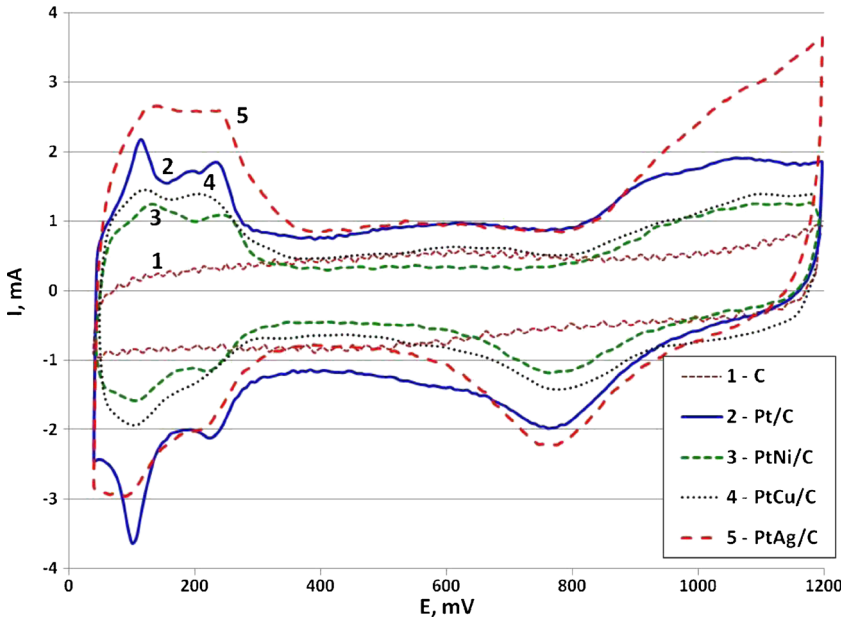

Fig. 2 Cyclic voltammograms of thin layer C(1), Pt/C(2), PtNi/C(3), PtCu/C(4), and PtAg/C (5) electrodes in 1 M H_2SO_4. The potential scan rate was 100 mV/s 5th cycle. Ar atmosphere

Table 4 Electrode characteristics of catalysts and their electrochemically active surface area as calculated by cyclic voltammetry results

Sample	Onset potential of CO oxidation, mV	Potential of peak's maximum of CO oxidation, mV	Electrochemically active surface area of the catalyst, m^2/g_{Pt-M} (the values in parentheses are related to the platinum weight, m^2/g_{Pt})		
			$ECSA^a$	$ECSA^{a+c}$	$ECSA^{CO}$
Pt/C	730±10	795±10	21	25	25
PtNi/C	740±20	810±20	21 (27)	20 (26)	16 (21)
PtCu/C	750±10	785±10	22 (29)	22 (29)	18 (24)
PtAg/C	895±10	940±10	39 (61)	43 (69)	39 (62)

The diffraction patterns of Pt/C, PtNi/C, and PtAg/C indicate the absence of any phases other than carbon, Pt, or platinum-based solid solutions (Pt-M) (Fig. 1, curves 1, 2, and 4). Weak copper (II) oxide peaks were observed in the PtCu/C diffraction patterns (Fig. 1a, curve 3; Table 2).

Note that the experimental metal loadings of all catalysts were close to the theoretical values calculated from the precursor amounts. The overall Pt:M ratios ignored the chemical state of the metals in the materials and also agreed with the theoretically predicted values. Calculation of the alloy composition was performed in accordance with Vegard's law under the assumption that metal nanoparticles are formed as solid solutions. The PtAg/C material was shown to form a solid solution, with a composition of approximately $Pt_{50}Ag_{50}$. For the PtNi/C catalyst and especially for the PtCu/C catalyst, the calculated concentration of the alloying component in the alloy was significantly lower than the concentration of Pt. There are some published data [21, 40–42] that indicate that the portion of the alloying component in Pt(M)-supported catalysts could be found in the amorphous oxides that decorate the nanoparticle surface. In accordance with the X-ray diffraction data (Table 1), copper is the most significant oxidized component of PtM/C catalysts that are prepared via wet synthesis. For PtCu/C, the platinum content of the alloy, as calculated by Vegard's law, is the highest compared to other the alloy catalysts, and a number of oxide peaks were observed in the diffraction pattern (Fig. 1a). Part of the nickel in the PtNi/C catalyst is in an amorphous[2] oxide and in a hydroxide state. EXAFS spectroscopy was employed to investigate the atomic interactions in the PtNi/C materials. Nickel atoms were confirmed to interact with other nickel atoms, platinum atoms, and with light carbon and/or oxygen atoms (Table 3). High nickel coordination numbers in relation to oxygen (carbon) (first coordinate sphere) (Table 3) indicate that part of the nickel in the catalyst is in an oxidized state. Considering the high coordination numbers of the platinum atoms in the PtNi/C catalyst, the Pt generally forms platinum–platinum and platinum–nickel bonds, and the platinum oxide bonds are weak (Table 3).

The scope of this work does not allow for a detailed analysis of the EXAFS data. Nevertheless, these results confirm the existence of a complex PtNi nanoparticle composition; there is no crystallized nickel oxide/hydroxide in the material, and an intermediate nickel–carbon layer can form at the nanoparticle/support boundary.

Silver has the highest (after platinum) standard electrode potential value and is negligibly oxidized during synthesis. According to the X-ray diffraction data (Table 2), this property enhances the alloying efficiency of the Pt–Ag system.

The cyclic voltammograms for the synthesized catalysts are typical for platinum dispersed on a carbon support (Fig. 2).

CV for platinum free carbon support is shown at the Fig. 2 for the comparison (Fig. 2, curve 1). One effect of this support is exhibited when the cathodic and anodic currents in the double layer region relative to those for platinized platinum are increased [1, 7, 43]. The characteristic peaks in the hydrogen area of the CV that correspond to various forms of adsorbed hydrogen are most pronounced on the Pt/C electrode (Fig. 2). The oxygen reduction peak potential in the CV cathodic branch is practically independent of the electrode material composition, whereas the value of the maximum current increases in the order of PtNi/C<PtCu/C<Pt/C<PtAg/C. Note that higher rates of Faraday (the hydrogen and oxygen regions of the CV) and non-Faraday (the double layer area of the CV) processes for the PtAg/C electrode were observed under almost all potential ranges.

[2] The Ni content in the Pt–Ni alloy as calculated using Vegard's low is less than the calculated value. However, there are no nickel oxide/hydroxide reflections in the XRD patterns of the PtNi/C sample. This result suggests that the nickel oxide/hydroxide, which contains a portion of the metal in the PtNi/C, is in an amorphous state.

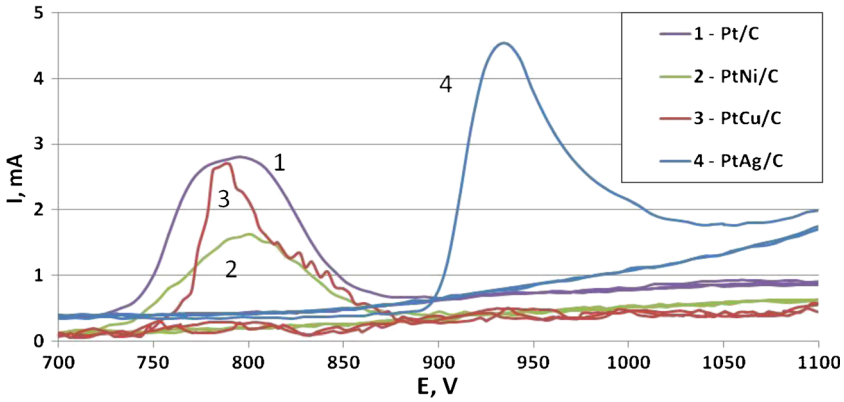

Fig. 3 Cyclic voltammogram cycles containing electrochemical desorption peaks for CO from the surface of catalyst nanoparticles. 1 M H_2SO_4. The potential scan rate was 40 mV/s. *1* Pt/C, *2* PtNi/C, *3* PtCu/C, *4* PtAg/C

The shape of the CV anodic branch in the oxygen region for this electrode also differed considerably; the anodic current rapidly increased as the potential shifted from 880 to 1200 mV, whereas for other PtM/C electrodes, an increase in the reaction rate and its stabilization were caused by the successive formation of various pre-phase platinum oxides [43].

It would be logical to hypothesize that the current increase results from the selective dissolution of silver from the alloy. However, the cyclic voltammogram parameters measured

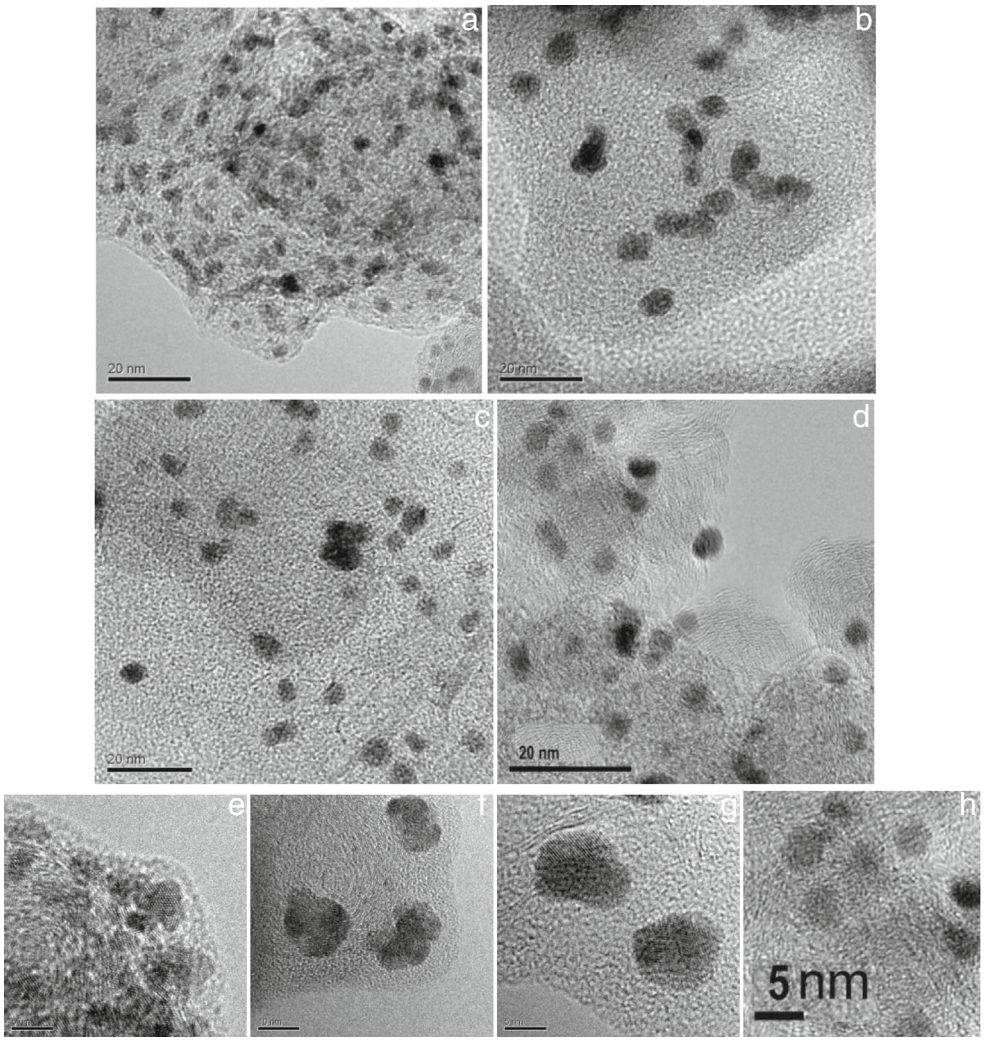

Fig. 4 Transmission electron microscopy of nanostructured catalysts: **a**, **e** Pt/C, **b**, **f** PtNi/C, **c**, **g** PtCu/C, and **d**, **h** PtAg/C

after standardizing the electrode surface were reproducible for 24 cycles (from the 2nd to the 25th cycle), whereas the current should decrease as the number of cycles increase because of the dissolution of silver and the subsequent diffusion of Ag^+ ions in the solution.[3] The peak observed in the cathodic branch of the CV oxygen area is associated with the reduction of oxygen chemisorbed on platinum, and there are no peaks related to the reduction of other products. Therefore, the rapid current increase in the anodic CV branch from the oxygen area could not be explained by the oxidation of silver accompanied by the formation of a surface oxide or sulfate. Considering the significantly higher currents in the anodic region of the CV hydrogen area, which are also typical for PtAg/C electrodes, the high rate of anodic reactions at potentials above 880 mV could be easily explained by the large surface areas of PtAg nanoparticles and by a change in the passivating properties of chemisorbed oxygen layers compared to those for other electrodes.

The calculated ECSA values for the studied electrocatalysts (Table 4), which were obtained from the hydrogen area of the CV and by the CO desorption method, revealed that the ECSA values for the PtAg/C catalyst are two or more times greater than those for other investigated materials.

Notably, the electrochemical desorption of CO from the surface of the PtAg/C electrode nanoparticles was considerably limited compared to other catalysts; the onset potentials and the maximum potential rate of CO oxidation were shifted to greater values by 120–150 mV (Table 4; Fig. 3). Because CO is minimally chemisorbed on silver [44, 45], the attempt to relate the ECSA to the surface (and amount) of platinum on the electrode appears to be correct. The ECSA value for the PtAg material was approximately 62 $m^{2*}g^{-1}_{(Pt)}$, which was 2.5–3 times more than similar values calculated for other electrodes (Table 4).

The ECSA values calculated for various catalysts from the CV hydrogen area ($ECSA^{a+c}$), from the anodic portion of the CV hydrogen area ($ECSA^{a}$), and from the peak CO desorption ($ECSA^{CO}$) (Table 3) poorly correlate with the average crystallite size (D_{av}). Considering the D_a values and knowing that the metal loading values for the various catalysts are identical (Table 2), the ECSA values of these materials should increase from PtAg/C<PtCu/C≈Pt/C<PtNi/C. However, the active surface area of these materials actually increases from PtNi/C≈PtCu/C<Pt/C<PtAg/C (Table 4). Thus, the relationship

[3] The initial cyclic voltammograms for the as-prepared PtAg/C catalyst in 0.5 M H_2SO_4 exhibit anodic and cathodic peaks at potential ranges of 0.64–0.70 and 0.45–0.52 V, respectively. Similar peaks were detected for Ag/C in the same solution. The intensities of these peaks for the as-prepared PtAg/C catalyst reduce as the number of cycles increases. We hypothesize that the behaviors of these peaks are associated with the dissolution of silver and the subsequent electroreduction (in the cathodic part of the cycle) of previously formed silver sulfate. There are no such peaks in the CVs for the standardized PtAg/C catalyst.

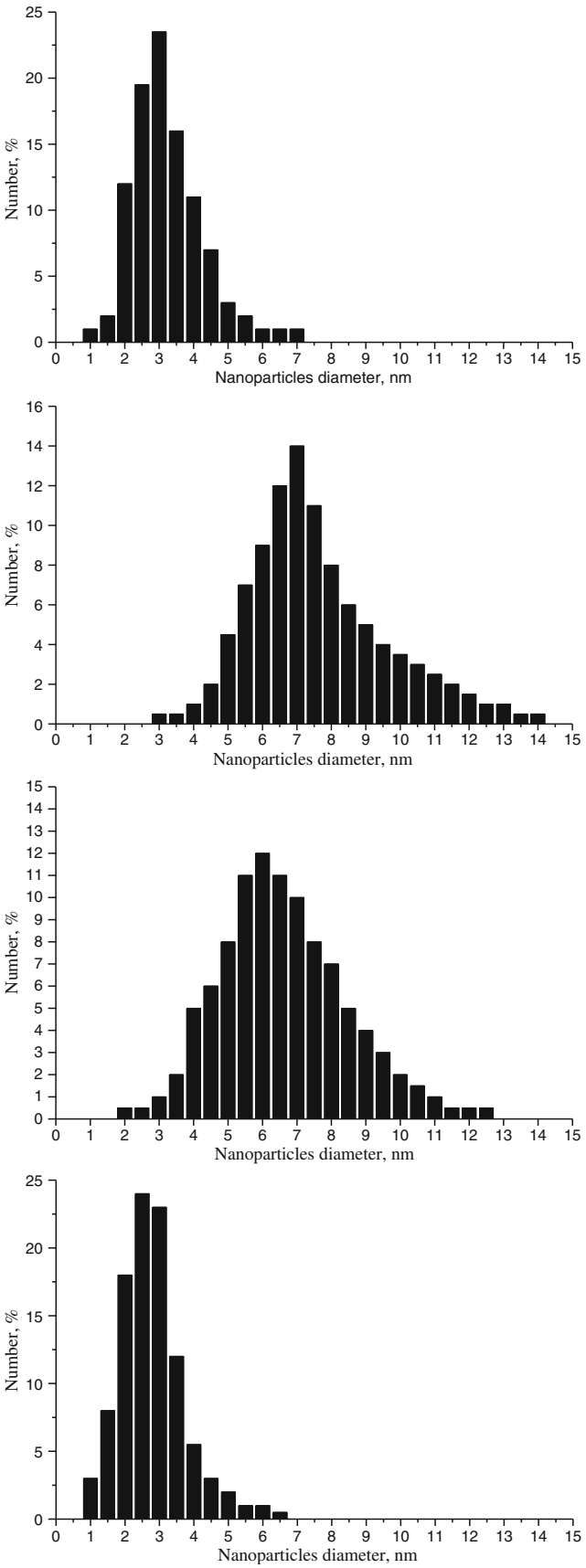

Fig. 5 Histograms of nanoparticle size distributions by TEM. **a** Pt, **b** PtNi, **c** PtCu, and **d** PtAg

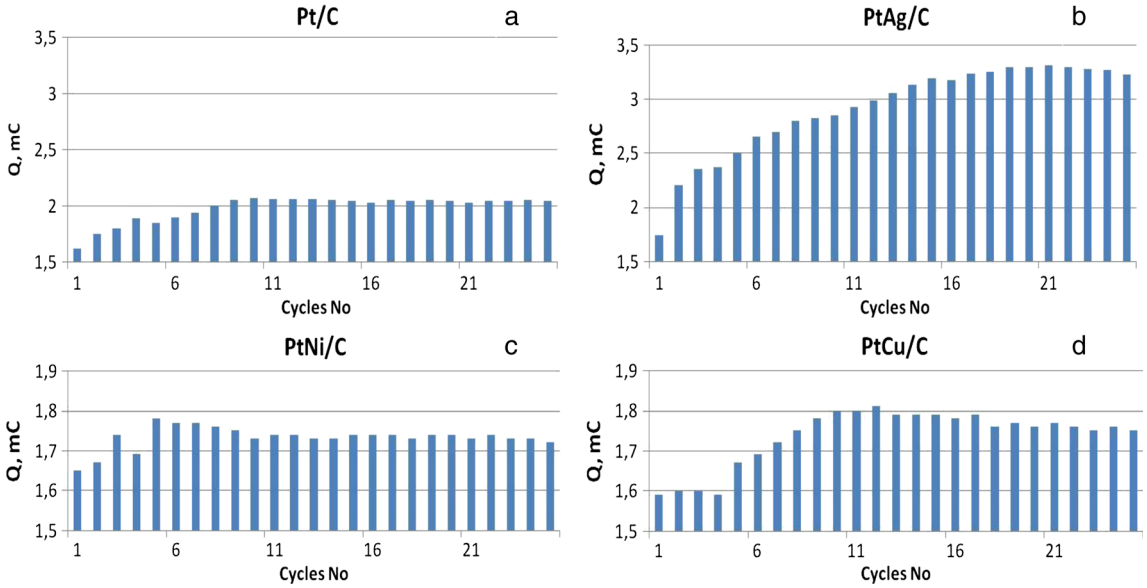

Fig. 6 Changes in the quantity of electricity consumed for the electrochemical desorption of hydrogen during preliminary thin-layer Pt/C (**a**), PtAg/C (**b**), PtNi/C (**c**), and PtCu/C (**d**) electrode cycling in 1 M H_2SO_4 (from cyclic voltammetry results)

between the average crystallite size estimated by XRD and the electrochemically active surface area of the metal is ambiguous.

In the case of PtM/C catalysts, the surface area value ratios, which were calculated using the crystallite size and measured using electrochemical techniques, also depended on the nature of the alloying component. The investigated catalysts can be divided into two groups as follows: materials with metallic nanoparticles (Pt/C and PtAg/C) and materials for which the surfaces of the metallic nanoparticles were significantly covered by oxide/hydroxide compounds of the alloying components (PtCu/C and PtNi/C). For the second group of catalysts, a portion of the metallic nanoparticle surface could be insulated by the oxides. It is necessary to account for the fact that nanoparticles and crystallites may not be identical to each other. As noted above, nanoparticles may consist of larger or smaller quantities of crystallites. A uniform nanoparticle spatial distribution and the degree of their agglomeration could depend on their composition.

A transmission electron microscopy investigation of the prepared electrocatalysts was performed to directly compare the sizes of the nanoparticles. The nanoparticle shapes were observed to be generally isotropic for all of the prepared materials (Fig. 4). The average nanoparticle sizes estimated by TEM were 7 nm (PtNi), 6 nm (PtCu), 3 nm (Pt), and 2.7 nm (PtAg). For PtNi, PtCu, and Pt, these values were larger than the crystallite sizes estimated by XRD. The nanoparticle sizes decreased in the following order: PtNi≥PtCu>Pt≥PtAg, and they did not correspond to the results of the XRD study, which showed decreasing average crystallite sizes as follows: PtAg/C>PtCu/C≈Pt/C>PtNi/C. The cause of this apparent mismatch can be explained as follows. In accordance with the TEM results together with isotropically shaped nanoparticles, nanoparticles with a more complex shape were observed among the investigated materials (Fig. 4e–i). Apparently, some of these nanoparticles corresponded to splices of unoriented crystallites.[4] To a great extent, this phenomenon was typical for PtNi and PtCu (Fig. 4f, g), and to a lesser extent, it was applicable to PtAg (Fig. 4h).

Thus, the lower ECSAs of the PtNi/C and PtCu/C catalysts relative to the Pt/C and PtAg/C catalysts were caused by larger PtNi and PtCu nanoparticles, a significant portion of which consisted of several aggregated crystallites (Figs. 4 and 5). Apparently, for PtNi nanoparticles, we cannot completely exclude the possibility of partial surface isolation by nickel oxide.

The larger ECSA of the PtAg/C catalyst relative to that of the Pt/C catalysts is caused by its smaller nanoparticle sizes and a lower extent of crystallite agglomeration (Figs. 4 and 5). The narrow nanoparticle size distribution, which is a characteristic of PtAg alloys (Fig. 5), also positively influences the ECSA value.

The differences among the ECSA values established for PtAg/C and for other studied electrocatalysts becomes even more significant if their calculation relates to the Pt mass unit (Table 2). This trend can be attributed to several causes. First, the PtAg alloy contains a smaller quantity of platinum (64.4 %) compared to the three investigated bimetallic systems. Therefore, the mass of platinum is minimal in a PtAg/C

[4] An assembly of crystallites can exceed the formation of isotropic nanoparticles, but at the initial stages of the transformation, we could expect the formation of nanoparticles with more complex shapes.

electrode at similar metallic component loadings in the catalysts. Moreover, the segregation of Pt atoms in surface alloy nanoparticle layers is apparently more typical for a PtAg alloy, which causes effective CO adsorption (Table 2).

As noted above, CO is weakly adsorbed on the surface of silver [44, 45], and the amount of chemisorbed and subsequently desorbed CO on the investigated PtAg/C nanoparticles was rather large (Fig. 3). The shape of the cyclic voltammograms obtained for the standardized PtAg/C catalysts was typical for platinum. This finding provides indirect evidence for high surface concentrations of platinum.

The estimated charges corresponding to the region of electrochemical hydrogen desorption (Q_a^H) on various electrodes over the course of their standardization, i.e., during preliminary cycling, are shown in Fig. 6. For the PtAg/C electrode, the charge consumed for the electrochemical desorption of hydrogen increases the most significantly and becomes stable later (after a larger number of cycles) compared to the other investigated electrodes (Fig. 6).

This result can be caused by a more pronounced and continuous increase in the surface concentration of platinum in relation to the selective dissolution of silver atoms. Note that the literature shows [42, 46] that the segregation of platinum atoms in the surface layer of nanoparticles is typical to a greater or lesser extent for solid solutions with different compositions and different alloying components.

Conclusions

This investigation of the microstructures and electrochemically active surface areas of Pt/C and PtM/C (M=Ni, Cu, Ag) electrocatalysts has revealed a number of factors that caused elevated ECSA values for the PtAg/C catalyst. The differences for the PtAg/C catalyst relative to the other studied materials were caused by the following factors:

- Small nanoparticle size (in comparison to PtCu and PtNi)
- Pronounced surface segregation of Pt in nanoparticles
- Weak aggregation and narrow size distribution of nanoparticles
- Reduced total weight concentration of Pt in the alloy

The actual composition of bimetallic particles corresponded to the theoretical (1:1) composition for the PtAg/C catalysts, whereas in the as-prepared PtNi/C and PtCu/C materials, part of the alloying component existed in an oxide form.

A determination of the average crystallite size by XRD did not provide sufficient criteria for estimating the catalyst microstructure. This information could not account for the formation of nanoparticles from some of the crystallites (PtNi and PtCu nanoparticles) or for the different aggregation extents for nanoparticles with different compositions.

The effects of adding Ag to the Pt/C catalysts could be of interest for controlling the microstructures and activities of Pt/C catalysts.

Acknowledgments This work was supported by the Russian Foundation for Basic Research (grants 10-03-00474a, 11-08-00499a) and by the Ministry of Education and Science of Russia (grants no. 14.740.11.0371 and 14.132.21.1468).

References

1. Bagotsky VS (2012) Fuel Cells: Problems and Solutions. 2nd ed. Wiley & Sons, 394 p
2. Perez J, Gonzalez ER, Ticianelli EA (1998) Oxygen electrocatalysis on thin porous coating rotating platinum electrodes. Electrochim Acta 44:1329–1339
3. Mayrhofer KJ, Blizanac BB, Arenz M, Stamenkovic VR, Ross PN, Markovic NM (2005) The impact of geometric and surface electronic properties of Pt-catalysts on the particle size effect in electrocatalysis. J Phys Chem B 109:14433–14440
4. Min M, Cho J, Cho K, Kim H (2000) Particle size and alloying effects of Pt-based alloy catalysts for fuel cell applications. Electrochim Acta 45:4211–4217
5. Tian N, Zhou ZY, Sun SG (2008) Platinum metal catalysts of high-index surfaces: from single-crystal planes to electrochemically shape-controlled nanoparticles. J Phys Chem C 112:19801–19817
6. Stamenkovic VR, Mun Bongjin S, Arenz M, Mayrhofer KJ, Lucas Christopher A, Guofeng W, Ross Philip N, Markovic NM (2007) Trends in electrocatalysis on extended and nanoscale Pt-bimetallic alloy surfaces. Nat Mater 6:241–247
7. Gasteiger HA, Kocha SS, Bhaskar S, Wagner FT (2005) Activity benchmarks and requirements for Pt, Pt-alloy, a reduction catalysts for PEMFCs. Appl Catal B Environ 56:9–35
8. Antolini E (2007) Catalysts for direct ethanol fuel cells. J Power Sources 170:1–12
9. Antolini E (2003) Formation, microstructural characteristics and stability of carbon supported platinum catalysts for low temperature fuel cells. J Mater Sci 38:2995–3005
10. Stamenković V, Schmidt TJ, Ross PN, Marković NM (2003) Surface segregation effects in electrocatalysis: kinetics of oxygen reduction reaction on polycrystalline Pt_3Ni alloy surfaces. J Electroanal Chem 554–55:191–199
11. Noel K, Xin W (2008) Pt-shell-Au-core/C electrocatalyst with a controlled shell thickness and improved Pt utilization for fuel cell reactions. Electrochem Commun 10:12–15
12. Hua LM, Shan DJ (2009) Kinetics of oxygen reduction reaction on Co_{rich} core–Pt_{rich} shell/C electrocatalysts. J Power Sources 188:353–358
13. Guofeng W, Van Hove MA, Ross PN, Baskes MI (2005) Quantitative prediction of surface segregation in bimetallic Pt–M alloy nanoparticles (M=Ni, Re, Mo). Review. Prog Surf Sci 79:28–45
14. Minhua S, Kotaro S, Marinkovic Nebojsa S, Lihua Z, Adzic Radoslav R (2007) Synthesis and characterization of platinum monolayer oxygen-reduction electrocatalysts with Co–Pd core–shell nanoparticle supports. Electrochem Commun 9:2848–2853
15. Chen Z, Deng W, Wang X, Yan Y (2007) Durability and activity study of single-walled, double-walled and multi-walled carbon nanotubes supported Pt catalyst for PEMFCs. ECS Trans 11:1289–1299
16. Ferrando R, Jellinek J, Johnston RL (2008) Nanoalloys: from theory to applications of alloy clusters and nanoparticles. Chem Rev 108: 845–910

17. Park KW, Ahn KS, Nah YC, Choi JH, Sung YE (2003) Electrocatalytic enhancement of methanol oxidation at Pt-WOx nanophase electrodes and in-situ observation of hydrogen spillover using electrochromism. J Phys Chem B 107:4352–4355
18. Cordero-Borboa AE, Sterling-Black E, Gómez-Cortés A, Vázquez-Zavala A (2013) X-ray diffraction evidence of the single solid solution character of bi-metallic Pt-Pd catalyst particles on an amorphous SiO2 substrate. Appl Surf Sci 220:169–174
19. Alegre C, Galvez ME, Baquedano E, Moliner R, Pastor E, Lazaro MJ (2013) Oxygen-functionalized highly mesoporous carbon xerogel-based catalysts for direct methanol fuel cell anodes. J Phys Chem C 117:13045–13058
20. Salgado JRC, Antolini E, Gonzalez ER (2004) Pt-Co/C electrocatalysts for oxygen reduction in H_2/O_2 PEMFCs synthesized by borohydride. J Electrochem Soc 151:A2143–A2149
21. Guterman VE, Pustovaya LE, Guterman AV, Vysochina LL (2007) Borohydride synthesis of the Ptx–Ni/C electrocatalysts and investigation of their activity in the oxygen electroreduction reaction. Russ J Electrochem 43:1091–1096
22. Guterman VE, Belenov SV, Dymnikova OV, Lastovina TA, Konstantinova YB, Prutsakova NV (2009) Influence of water-organic solvent composition on composition and structure of Pt/C and Pt_xNi/C electrocatalysts in borohydride synthesis. Inorg Mater 45:498–505
23. Guterman AV, Pakhomova EB, Guterman VE, Kabirov YV, Grigor'ev VP (2009) Synthesis of nanostructured PtxNi/C and PtxCo/C catalysts and their activity in the reaction of oxygen electroreduction. Inorg Mater 45:767–772
24. Guterman VE, Pakharev AY, Tabachkova NY (2013) Microstructure and size effects in Pt/C and Pt3Ni/C electrocatalysts synthesized in solutions-based on binary organic solvents. Appl Catal A Gen 453:113–120
25. Schulenburg H, Durst J, Müller E, Wokaun A, Scherer GG (2010) Real surface area measurements of Pt_3Co/C catalysts. J Electroanal Chem 642:52–60
26. Colmenares L, Guerrini E, Jusys Z, Nagabhushana KS, Dinjus E, Behrens S, Habicht W, Bonnemann H, Behm RJ (2007) Activity, selectivity, and methanol tolerance of novel carbon-supported Pt and Pt_3Me (Me=Ni, Co) cathode catalysts. J Appl Electrochem 37:1413–1427
27. Yang H, Coutanceau C, Le ger JM, Alonso-Vante N, Lamy C (2005) Methanol tolerant oxygen reduction on carbon-supported Pt–Ni alloy nanoparticles. J Electroanal Chem 576:305–313
28. Hui Y, Vogel W, Lamy C, Alonso-Vante N (2004) Structure and electrocatalytic activity of carbon-supported Pt-Ni alloy nanoparticles toward the oxygen reduction reaction. J Phys Chem B 108:11024–11034
29. Qinghong H, Hui Y, Yawen T, Tianhong L, Akins DL (2006) Carbon-supported Pt–Co alloy nanoparticles for oxygen reduction reaction. Electrochem Commun 8:1220–1224
30. Venkateswara Rao C, Javier P, Ghatty Sundara L, Rambabu B (2010) High-temperature polymer electrolyte membrane fuel cell performance of Pt_xCoy/C cathodes. J Power Sources 195:3425–3430
31. Vidaković T, Christov M, Sundmacher K (2007) The use of CO stripping for in situ fuel cell catalyst characterization. Electrochim Acta 52:5606–5613
32. Jue H, Chengxu Z, Lin J, Yuedong M (2013) Morphology controlled synthesis and characterization of vertically aligned carbon nanofibers supported platinum catalysts for polymer electrolyte fuel cells. J Phys Chem C 117:12902–12908
33. T Roisnel, J Rodriguez-Carvajal, (2000) WinPLOTR: a Windows tool for powder diffraction patterns analysis. Materials Science Forum, Proceedings of the Seventh European Powder Diffraction Conference (EPDIC 7): 118-123
34. Leontyev IN, Chernyshov DY, Guterman VE, Pakhomova EV, Guterman AV (2009) Particle size effect in carbon supported Pt–Co alloy electrocatalysts prepared by the borohydride method: XRD characterization. Appl Catal A 357:1–4
35. Leontyev IN, Belenov SV, Guterman VE, Haghi-Ashtiani P, Shaganov AP, Dkhil B (2011) Catalytic activity of carbon supported Pt/C nano-electrocatalysts. Why reducing the size of Pt nanoparticles is not always beneficial. J Phys Chem C 115:5429–5434
36. Leontyev IN, Guterman VE, Pakhomova EB, Timoshenko PE, Guterman AV, Zakharchenko IN, Petin GP, Dkhil B (2010) XRD and electrochemical investigation of particle size effects in platinum–cobalt cathode electrocatalysts for oxygen reduction. J Alloys Compd 500:241–246
37. Chernyshov AA, Veligzhanin AA, Zubavichus YV (2009) "Structural materials science" end-station at the Kurchatov synchrotron radiation source: recent instrumentation upgrades and experimental results. Nucl Instr Meth Phys Res A 603:95–98
38. Newville M (2001) EXAFS analysis using FEFF and FEFFIT. JSynchrotron Radiat 8:322–324
39. Zabinski SI, Rehr JJ, Ankudinov A, Albers RC, Eller MJ (1995) Multiple-scattering calculations of X-ray absorption spectra. Phys Rev B 52:2995–3009
40. Antolini E, Salgado Jose RC, Gonzalez Ernesto R (2006) Oxygen reduction on a $Pt_{70}Ni_{30}/C$ electrocatalyst prepared by the borohydride method in H_2SO_4/CH_3OH solutions. J Power Sources 155:161–166
41. Lima FHB, Lizcano-Valbuena WH, Teixeira-Neto E, Nart FC, Gonzalez ER, Ticianelli EA (2006) Pt-Co/C nanoparticles as electrocatalysts for oxygen reduction in H_2SO_4 and H_2SO_4/CH_3OH electrolytes. Electrochim Acta 52:385–752
42. Bogdanovskaya VA, Tarasevich MR, Reznikova LA, Kuznetsova LN (2010) Composition, surface segregation, and electrochemical properties of binary PtM/C (M=Co, Ni, Cr) catalysts. Russ J Electrochem 46:1011–1020
43. Damaskin BB, Petrii OA, Tsirlina GA (2001) In: Electrochemistry. Khimiya, Moscow
44. Rincón A, Pérez MC, Orozco G, Gutiérrez C (2001) Test of the water adsorption model of organic electrocatalysis in the carbon monoxide-silver system in alkaline medium. Electrochem Commun 3:357–362
45. Cuesta A, López N, Gutiérrez C (2003) Electrolyte electroreflectance study of carbon monoxide adsorption on polycrystalline silver and gold electrodes. Electrochim Acta 48:2949–2956
46. Paulus UA, Wokaun A, Scherer GG, Schmidt TJ, Stamenkovic V, Radmilovic V, Markovic NM, Ross PN (2002) Oxygen reduction on carbon supported Pt-Ni and Pt-Co alloy catalysts. J Phys Chem B 106:4181–4191